Electronic Supplementary Material (ESI) for Environmental Science: Nano.
This journal is © The Royal Society of Chemistry 2023

Supplementary Information

Dissolved Organic Matter Regulates Aggregation and Deposition of Chromium (Hydr)oxide Colloids: Molecular-Scale Investigation Using ESI-FT-ICR-MS

Shishu Zhu, [a] *Yijun Mo,* [a] *Wendan Luo,* [a] *Zihan Xiao,* [a] *Chao Jin,* [*, a] *Rongliang Qiu* [a, b]

[a] School of Environmental Science and Engineering, Guangdong Provincial Key Laboratory of Environmental Pollution Control and Remediation Technology, Sun Yat-sen University, Guangzhou 510275, P. R. China

[b] Guangdong Laboratory for Lingnan Modern Agriculture, Guangdong Provincial Key Laboratory of Agricultural & Rural Pollution Abatement and Environmental Safety, College of Natural Resources and Environment, South China Agricultural University, Guangzhou 510642, China

---

***Corresponding Author:**

Chao Jin, Sun Yat-sen University,

E-mail: jinchao3@mail.sysu.edu.cn

Contents:

Cr_2O_3 and (b) $Cr(OH)_3$ in the presence of DOM.

Figure S10. The dynamic changes in hydrodynamic diameters (nm) of (a) $Cr(OH)_3$ and (b) Cr_2O_3 under different DOM loadings (mg C L^{-1}). Schematic representation of corona formation of Cr (hydr)oxides and its impacts on the colloidal stabilities. The organic compound formulas were only shown to illustration.

Figure S11 DLVO calculation profiles of Cr (hydr)oxide colloids with SDOM: (a-b) colloid-surface, (c-d) colloid-colloid.

Figure S12. Deposition kinetics of Cr (hydr)oxide colloids with or without DOM detected in a QCM-D system.

Figure S13. Deposition irreversibility (detachment efficiencies) (%) of $Cr(OH)_3$ and Cr_2O_3 in a QCM-D system as a function of DOM loadings (mg C L^{-1}).

Text S1. Chemicals and materials

Crystalline Cr oxides, Cr_2O_3 (> 99.0%, CAS: 1308-38-9), was purchased from Shanghai Macklin Biochemical, Co., Ltd. Chromium hydroxide ($Cr(OH)_3$) was obtained from Strem Chemicals, INC. Other chemical agents were purchased from Aladdin, Co., Ltd. Milli-Q water was used for all solutions. Solid samples were ground and then dissolved in solution to allow them to sediment for 24 h. When the sedimentation was complete, the supernatants as colloids were siphoned. Such processes were repeated for three times and the collected supernatants were stored as colloid stock solution in dark. Colloid concentration was measured via freeze-drying the constant volume of stock solution and weighing the dried solids. Constant colloid concentration of 1000 mg L^{-1} was applied for following experiments by diluting the colloid stock solution with known concentration. X-ray diffractometer (XRD, Ultima IV, Rigaku, Japan) was used to identify the crystalline phases of the three Cr-containing colloids. Each data profile was obtained within 2θ angles between 10° and 90°. Porosity and surface area were tested using a surface-area pore analyzer (ASAP2460, Micromeritics, USA). Transmission electron microscope (TEM, Talos F200s, FEI, USA) was used to observe the morphology features of Cr (hydr)oxide colloids. Density of surface protonated hydroxyl groups on Cr-colloids were determined as previous reports. [1, 2] An acid-base titration method was used to determine the surface hydroxyl content of Cr (hydr)oxides. Briefly, the constant mass of Cr (hydr)oxides was first neutralized by NaOH solutions, then NaOH supernatant was titrated with a standard HNO_3 solution after filtrating the solid phases. Density of surface hydroxyl groups can be calculated from the base consumption.

Sample was obtained from the topsoil in a paddy field (0-20 cm depth) at Heilong Jiang province, China. Samples were air-dried and stored at the room temperature in the laboratory. DOM Extraction method can be found in previous studies. [3, 4] Briefly, the solid suspensions (50 g soil diluted to 1000 mL water) were shaken for more than 48 h, following centrifuged for 30 min and filtered through 0.45 μm membrane. PPL cartridges and HPLC methanol were used to purify the extracted DOM. The extracted DOM sample was stored in a glass vital (in dark condition) at 4 °C and used within one week.

Text S2. Modified Langmuir Model

Based on the previous study, [5] the adsorption of DOM on mineral colloids followed a modified Langmuir model. Briefly, this model was reformulated with the incorporation of a correction factor, $(C/C_a)^h$, which described the nonequilibrium desorption hysteresis:

$$\frac{\partial \mathrm{q}}{\partial \mathrm{t}} = k_{\mathrm{f}} C\left(q_{\max} - q\right) - k_{\mathrm{b}} q\left(\frac{C}{C_{\mathrm{a}}}\right)^{h} \quad \text{eq. s1}$$

$$q = \frac{K_{\mathrm{q}} q_{\max} C}{K_{\mathrm{q}} C + \left(\frac{C}{C_{\mathrm{a}}}\right)^{h}} \quad \text{eq. s2}$$

where C and q was the aqueous concentration (mg L^{-1}) and solid DOM concentration (mg g^{-1}), C_a was the DOM equilibrium concentration after adsorption but before desorption occurred, h was the hysteresis coefficient, the K_f and q_{max} represented the adsorption affinity and theoretical maximum adsorption capacity. When h=0 and 1, the adsorption processes were completely reversible and irreversible, respectively. In this study, the q in the model corresponded to the normalized adsorption quantity ($Q_{s,N}$).

Text S3. Differentiating the contributions of different interactions

Impacts of background electrolytes (e.g., 0.01 M $CaCl_2$, 0.01 M NaCl, and 0.01 M NaCl-NaH_2PO_4) on adsorbed quantities of total organic carbon represented the contributions of binding mechanisms. [6, 7] Although the binding forces with DOM were complex, this empirical method provided the visualized and semiquantitative information using batch experiments. The methods in previous studies were employed under same conditions with our study. It is believed the approach was referential to process the results in the study. Based on the adsorbed quantities of DOM with different electrolytes, the contributions of van der Waals force (vdW), Ca^{2+} bridging (CB), and ligand exchange (LE) were calculated as followings:

$$f^{\mathrm{CB}} = \frac{Q_0\left(\mathrm{CaCl_2}\right) - Q_0(\mathrm{NaCl})}{Q\left(\mathrm{CaCl_2}\right)} \quad \text{eq. s3}$$

$$f^{\mathrm{LE}} = \frac{Q_0(\mathrm{NaCl}) - Q_0(\mathrm{NaCl - NaH_2PO_4})}{Q\left(\mathrm{CaCl_2}\right)} \quad \text{eq. s4}$$

$$f^{\mathrm{vdW}} = \frac{Q_0(\mathrm{NaCl - NaH_2PO_4})}{Q_0\left(\mathrm{CaCl_2}\right)} \quad \text{eq. s5}$$

where f^{CB}, f^{LE}, and f^{vdW} represent contributions (%) of different binding mechanisms; $Q_0(CaCl_2)$, Q_0 (NaCl), and Q_0 (NaCl-NaH_2PO_4) represented the adsorbed quantities of DOM at a certain aqueous DOM concentration in different electrolytes. According to the Q_0 values, the f^{vdW}, f^{CB}, and f^{vdW} at every

certain initial aqueous DOM concentration can be obtained.

Text S4. FT-ICR-MS measurement and data processing

Solid phase extraction using the Varian Bond Elute PPL cartridges (1 g per 6 mL) [8, 9] was employed to exclude the impact of inorganic ions and concentrate these DOM samples. The cartridges were rinsed with methanol and then used to extract the acidified samples (~50 mL with pH of 2). The cartridges were then rinsed using constant volumes of 0.01 M HCl and further dried in a N_2 atmosphere. After extracting the cartridges by methanol, the eluted solutions were dried and redissolved in methanol solution (methanol to water with 50:50, *v*/*v*) for FT-ICR-MS measurements. Equal mass concentration of the samples (~25 mg C L^{-1}) was used to reduce the concentration-induced differences in ionization efficiency. Extracted DOM samples were tested using a Bruker SolariX FT-ICR-MS (15.0 T super-conducting magnet and ESI ion source) as the procedures in previous studies. [1, 9] Flow rate of syringe infusion reached 120 μL h^{-1} and ESI voltage was set to be -3.8 kV. Samples were analyzed with negative ionization mode and ion accumulation time of 0.2 s. The mass error of an internal calibration kept less than 0.5 ppm. Bruker Data Analysis software was employed to explore the chemical formula assignments.

Three selection criteria are used herein: 1) signal-to-noise ratio (S/N) should be greater than 4; 2) elemental combinations are within range of $C_{5\text{-}80}H_{10\text{-}200}O_{0\text{-}40}N_{0\text{-}2}S_{0\text{-}2}$; and 3) the mass error between measured and calculated mass should be less than 500 ppb. van Krevelen diagram was established when H/C< 2.0 and O/C< 1.2. Parameters including H/C and O/C ratio, double bond equivalence (DBE), aromaticity index (AI), nominal oxidation state of carbon (NOSC) per molecule, and $FI_{O/C}$ were calculated. [11-13] Kendrick mass defect (KMD) analysis was employed to separate the assigned compounds as different homologous series group (e.g., -COO and -CH_2), [14] while the parameter of *I* was used to distinguish the relative adsorption affinity of multiple formulas. [15, 16] The DBE and AI were determined as:

$$DBE = 1 + \frac{2C - H + N}{2} \quad \text{eq. s6}$$

$$AI = \frac{1 + C - 0.5 \times O - 0.5 \times H - S}{C - 0.5 \times O - N - S} \quad \text{eq. s7}$$

Nominal oxidation state of carbon (NOSC), could be used to reflect the oxidation state or sequestering degree of carbon and determined as:

$$NOSC = 4 - \frac{4 \times C + H - 2 \times O - 3 \times N - 2 \times S + 5 \times P}{C} \quad \text{eq. s8}$$

Furthermore, the number-averaged values of C_w, H_w, O_w, H/C_w, DBE_w for assigned compounds were calculated.

Kendrick mass defect (KMD) analysis [16] was used to represent different homologous series of assigned compounds. These homologous series only differed in the number of a specific group but owned the same KMD of formulas. Kendrick mass of a specific compound was converted using IUPAC mass, while Kendrick mass defect (KMD) was determined as:

$$\text{Kendrick mass} = \text{Observed mass} \times \frac{\text{nominal mass}}{\text{exact mass}} \quad \text{eq. s9}$$

$$\text{Kendrick mass defect (KMD)} = \text{nominal mass} - \text{Kendrck mass} \quad \text{eq. s10}$$

where the IUPAC mass of $-CH_2$ and -COO group was assigned to be 14.01565 and 43.9898 Da, respectively. [15]

Based AI and H/C values, the compositions of DOM were classified into four categories: Group 1: condensed aromatics with polycyclic structures (AI > 0.67), Group 2: non-condensed vascular plant-derived polyphenols (0.67 ≥AI >0.5), Group 3: highly unsaturated and phenolic compounds (0.5 ≥AI, H/C< 1.5), and Group 4: less pronounced aliphatic compounds (2.0 ≥H/C ≥ 1.5).

The parameter *I* was used to describe the adsorption affinities of assigned compounds in homologous series. [15, 16] This approach provided the information about the extent of adsorption fractionation, rather than the adsorption quantity. In brief, parameter *I* could be determined by the ratio of the normalized peak intensity of compound ions in residual DOM after adsorption to those in original DOM. When the response intensities of assigned compounds rely on their concentrations and ionization efficiencies, the total quantity of a specific compound in DOM affected the normalized intensity in mass spectrum. It is defined that the assigned compounds with *I* value lower than 0.5 are highly well adsorbed, while those with values of *I* higher than 0.9 are not or poorly adsorbed. The compounds not existing in residual DOM after adsorption were regarded as quantitatively adsorbed groups ($I = 0$).

Text S5. DLS and QCM-D experiments

Changes in hydrodynamic diameter (D_h) of adsorbed Cr (hydr)oxides was tested using Time-resolved

dynamic light scattering (DLS, Zetasizer Nano). First, 1 mL Cr (hydr)oxide colloid suspension was first sonicated for 15 min and the colloids were mixed with DOM stock solution in the DLS cuvette to obtain desired DOM loading. The corvettes were immediately transferred into DLS cells and the continual changes in the average D_h were monitored at each 30s.

Deposition experiments were conducted using Quartz Crystal Microbalance with Dissipation (QCM-D) system (Q-Sense Explorer, Biolin Scientific AB, Sweden). Before deposition experiments, the crystal sensors (SiO_2, QSX 303) were preconditioned as followings: 1) UV/ozone treatment for 10 minutes; 2) immersing the sensor surfaces in the 2% Sodium Dodecyl Sulfate (SDS) solution for 30 min; 3) keeping wet surface and rinsing with Milli-Q water; 4) dried with nitrogen gas; 5) another 10–minute UV/ozone treatment. Flow rate into the flow chamber was controlled at 0.1 mL min^{-1} using a peristaltic pump (REGLO Digital ISM 596, ISMATEC, Switzerland). Prior to injecting samples, DI water was used as background fluid to stabilize the system until normalized third overtone frequency shift (Δf_3) was less than 0.3 Hz in 10 min. The Cr (hydr)oxide suspensions with or without DOM were injected into the chamber to obtain the Δf curve. In particular, the Cr (hydr)oxide samples were first mixed with DOM solution with a constant loading (mg C L^{-1}). Then the suspensions including the colloids and DOM were further injected into QCM-D system. With the deposition of Cr (hydr)oxide suspensions with or without DOM colloids on surfaces, the increased mass of the crystal sensor leads to a negative shift in the overtone frequencies (Δf_n). The direct relationship between the deposition mass (Δm) and the shift in frequencies could be described by the Sauerbrey equation. Ratios of ΔD to Δf were calculated to present the dissipated energy. [17]

$$\Delta m = -C \times \frac{\Delta f_n}{n} \qquad \text{eq. s11}$$

where n (1, 3, 5, 7⋯) is the overtone number and C is the crystal constant (17.7 ng Hz^{-1} cm^{-2}). Overtone number 3 was used in this study. Since the deposited mass of Cr (hydr)oxide suspensions with or without DOM onto collector surfaces is linearly related to the frequency change, the deposition rates can be indicated by the rates of frequency shift. Normalized frequency shifts monitored by QCM-D at the third overtone during early stage (∼1−3 min) were used to calculate the initial deposition rates (r_D) which was quantified as following: [18-19]

$$r_D = \frac{d\Delta f_n}{dt} \qquad \text{eq. s12}$$

Text S6. DLVO interaction

Nanoscale roughness has been demonstrated to significantly influence the prediction of interaction energy profiles of spherical colloids. [20-22] If pillars of nanoscale roughness are uniformly distributed on the smooth collector surface, the total interaction energy can be determined as: [22, 23]

$$\Phi(h) = (1 - f_r)\Phi_S(h + h_r) + f_r\Phi_S(h) \qquad \text{eq. s13}$$

where h_r [L, where L denotes units of length] and f_r [-]are the height of pillars in the zone and the roughness density, respectively, and h [L] is the separation distance. The interaction energy of Φ_s [ML^2/T^2, where M and T denote units of mass and time] for a spherical colloid and collector system was calculated as the sum of electrostatic, van der Waals, and Born repulsion interaction energies:

$$\Phi_S(h) = \Phi_s^{EDL}(h) + \Phi_s^{VDW}(h) + \Phi_s^{Born}(h) \qquad \text{eq. s14}$$

where Φ_s^{EDL} [ML^2/T^2], Φ_s^{VDW} [ML^2/T^2] and Φ_s^{Born} [ML^2/T^2] are the electrostatic, van der Waals, and Born interaction energies on the smooth surface, respectively. The value of Φ_s^{EDL} was determined using the constant surface potential interaction expression of Hogg et al. [24] for a sphere-plate interaction as:

$$\Phi_s^{EDL}(h) = \pi\varepsilon\varepsilon_0 r_c \left\{ 2\left[\frac{1+\exp(-\kappa h)}{1-\exp(-\kappa h)}\right] + (\zeta_1^2 + \zeta_2^2)\ln\left[1-\exp(-2\kappa h)\right]\right\} \qquad \text{eq. s15}$$

where ε (dimensionless) is the dielectric constant of the medium, ε_0 [$T^4/M\cdot L\cdot A$, $\zeta_1\zeta_2 ln$ where A denotes ampere] is the permittivity in a vacuum, r_c [L] is the radius of a colloid, h is the distance between colloid and quartz surface, ζ_1 is the zeta potential of the colloid, ζ_2 is the zeta potential of the collector, and κ [L^{-1}] is the Debye-Höckel parameter, which can be calculated as follows: [25]

$$\kappa = \sqrt{\frac{e^2 \sum n_{j0} z_j^2}{\varepsilon_0 \varepsilon\, K_B T}} \qquad \text{eq. s16}$$

where N_A is the Avogadro number (6.02×10^{23} mol^{-1}), e is the charge of the electron (-1.60×10^{-19} C), n_{j0} is the number concentration of ions in the bulk solution, z_j is the ion valence of the background electrolyte, K_B is the Boltzmann constant (1.38×10^{23} J/K), T is the absolute temperature (298 K). The

value of Φ_s^{VDW} for a sphere-plate interaction was determined using expression by Gregory as: [26]

$$\Phi_s^{VDW}(h) = -\frac{A_{132} r_c}{6h}\left[1+\frac{14h}{\lambda}\right]^{-1} \quad \text{eq. s17}$$

where A_{132} [ML^2/T^2] is the Hamaker constant, and λ [T] is a characteristic wavelength that was taken as 100 nm. [27] The value of Φ_s^{Born} was calculated from Ruckenstein and Prieve as: [28]

$$\Phi_s^{Born}(h) = \frac{A_{123}\sigma_c^6}{7560}\left[\frac{8r_c + h}{(2r_c+7)^7} + \frac{6r_c - h}{h^7}\right] \quad \text{eq. s18}$$

The collision diameter, σ_c, was taken as 0.26 nm in order to achieve a primary minimum depth at 0.157 nm, a commonly accepted distance of the closest approach. [29] Interactions between two colloids in suspension can be determined as follows: [26, 30]

$$\Phi_s^{EDL}(h) = \pi\varepsilon\varepsilon_0 \frac{a_{s1}a_{s2}}{a_{s1+}a_{s2}}\left\{2\zeta_{s1}\zeta_{s2}\left[\frac{1+\exp(-\kappa h)}{1-\exp(-\kappa h)}\right] + \left(\zeta_{s1}^2 + \zeta_{s2}^2\right)\ln\left[1-\exp(-2\kappa h)\right]\right\} \quad \text{eq. s19}$$

$$\Phi_s^{VDW}(h) = -\frac{A_{132} a_{s1} a_{s2}}{6h(a_{s1+}a_{s2)}}\left[1+\frac{14h}{\lambda}\right]^{-1} \quad \text{eq. s20}$$

where a_{s1} [L] and a_{s2} [L] represent the radius of the two colloids ζ_{s1} and ζ_{s2} represent the zeta potential of the two kinds of colloids. Here, h represents the distance between two colloids. The calculation of the Hamaker constant A_{132} is provided below.

Figures:

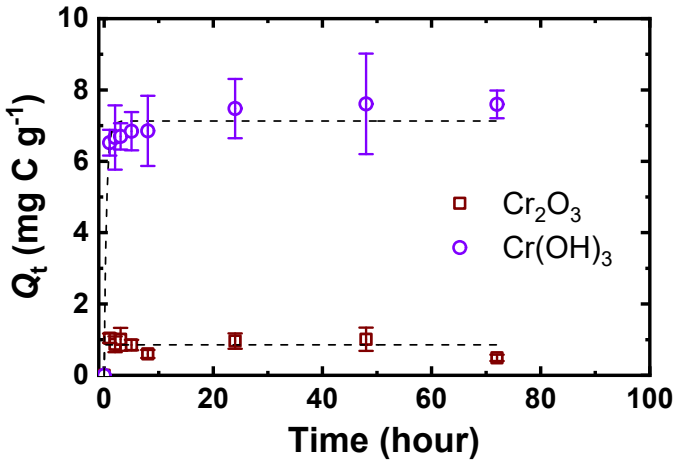

Figure S1. Adsorption kinetics of DOM on the $Cr(OH)_3$ and Cr_2O_3 within 72 hours.

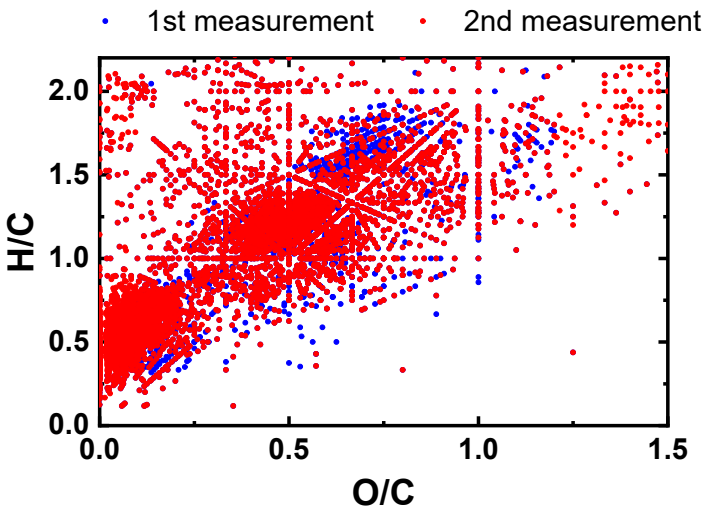

Figure S2. van Krevelen diagrams for original DOM detected using FT-ICR-MS. The blue spots that not overlapped with the red spots represented the differences. Duplicated measurements were less than 10% difference of assigned formulas.

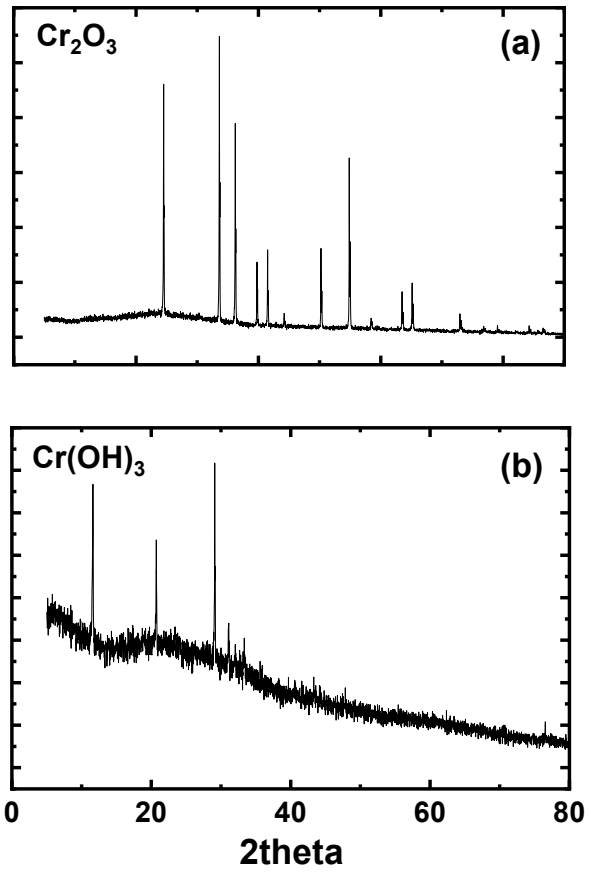

Figure S3. X-ray diffraction patterns of (a) Cr_2O_3 and (b) $Cr(OH)_3$.

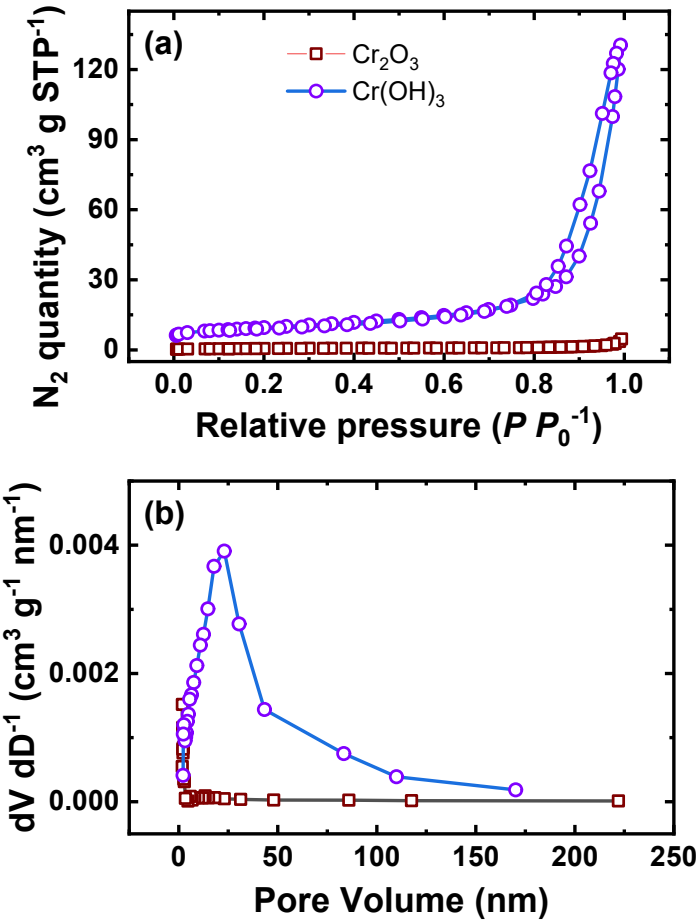

Figure S4. (a) N_2 adsorption/desorption curves at 77 K and (b) pore distributions of $Cr(OH)_3$ and Cr_2O_3.

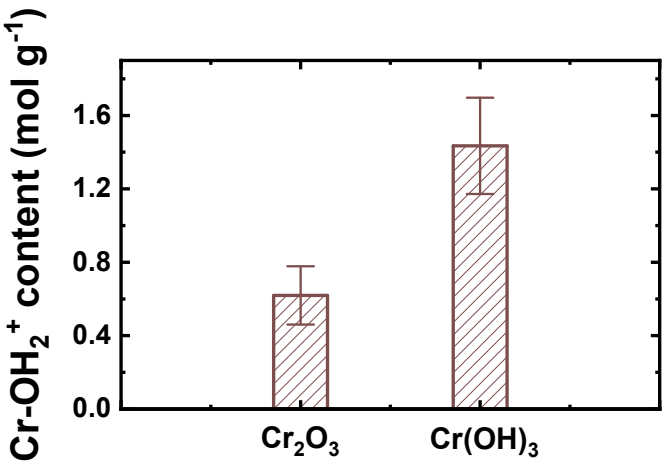

Figure S5. (a) Determination of surface reactive hydroxyl group contents (mol g^{-1}) on $Cr(OH)_3$ and Cr_2O_3.

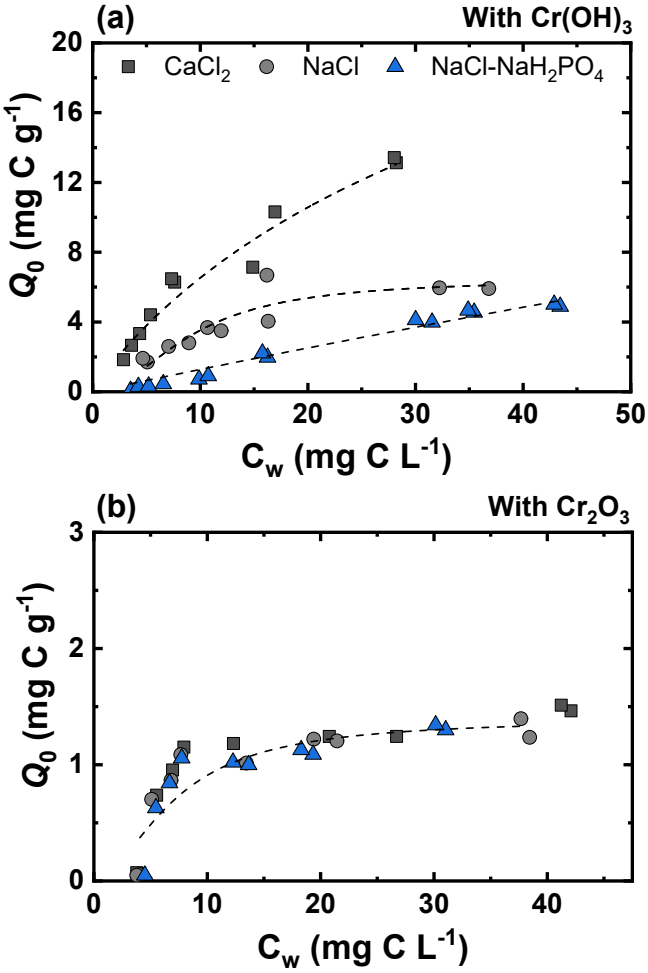

Figure S6 Adsorption isotherms of DOM on (a) $Cr(OH)_3$ and (b) Cr_2O_3 under different background electrolytes (i.e., 0.1 M $CaCl_2$, 0.1 M NaCl, and 0.01 M NaCl-NaH_2PO_4). The Q_0 (mg C g^{-1}) of DOM was used to determine the contributions of different binding mechanisms. Dashed line represented the fitting data using modified Langmuir model.

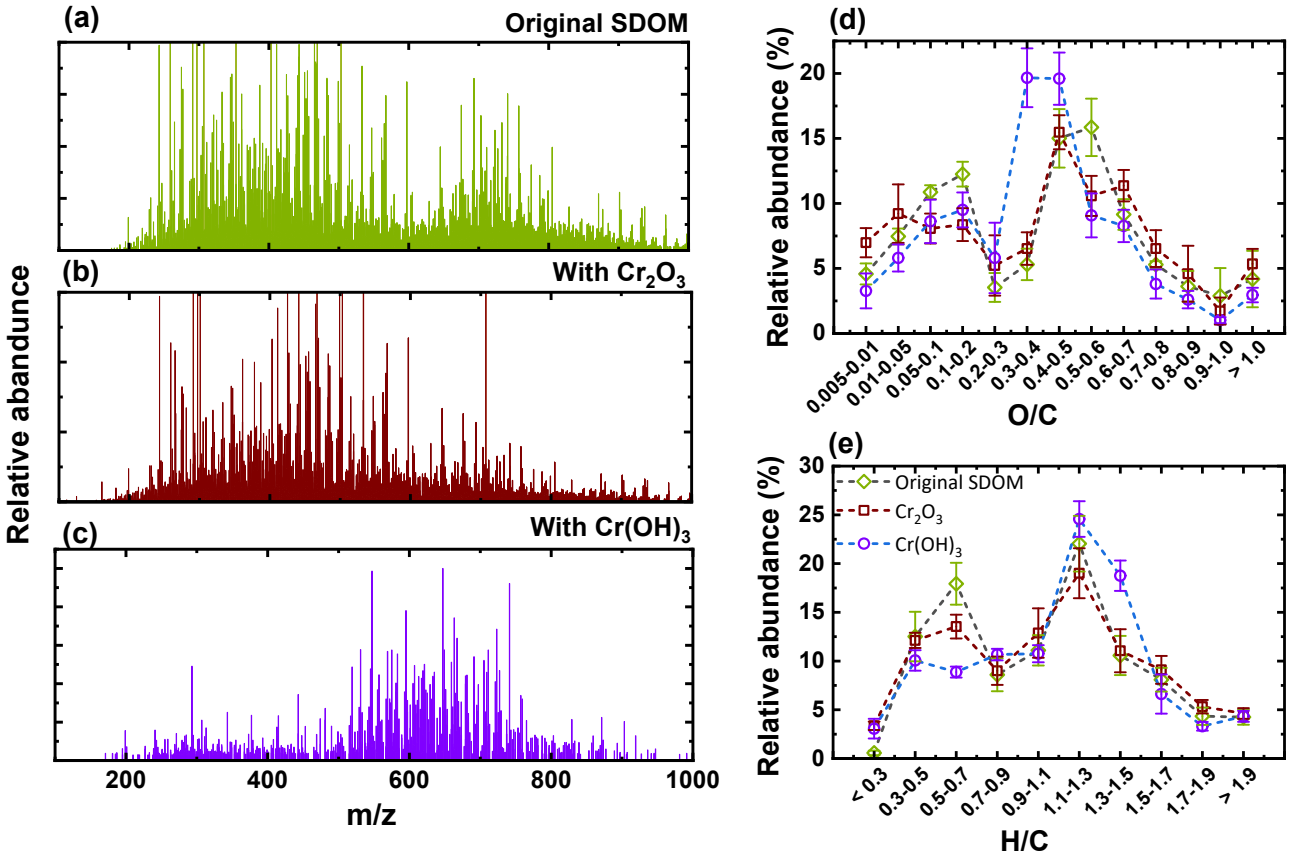

Figure S7 (a-c) FT–ICR–MS mass spectrum of detected formulas in original DOM or remaining DOM in the presence of $Cr(OH)_3$ and Cr_2O_3. The changes in relative abundance (%) of molecules as a function of (d) O/C and (e) H/C in the original DOM or remaining DOM in the presence of $Cr(OH)_3$ and Cr_2O_3.

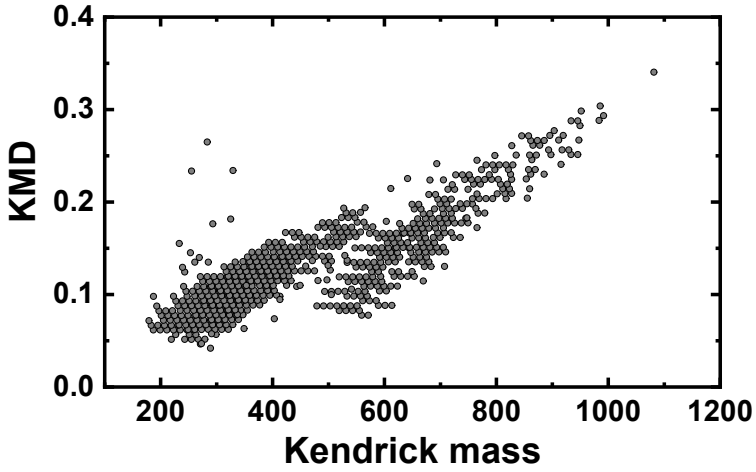

Figure S8 Kendrick mass defect of -COO homologous series that exhibited the affinities more than 0.5. The homologous series along the horizontal lines represented the mass difference of carboxylates.

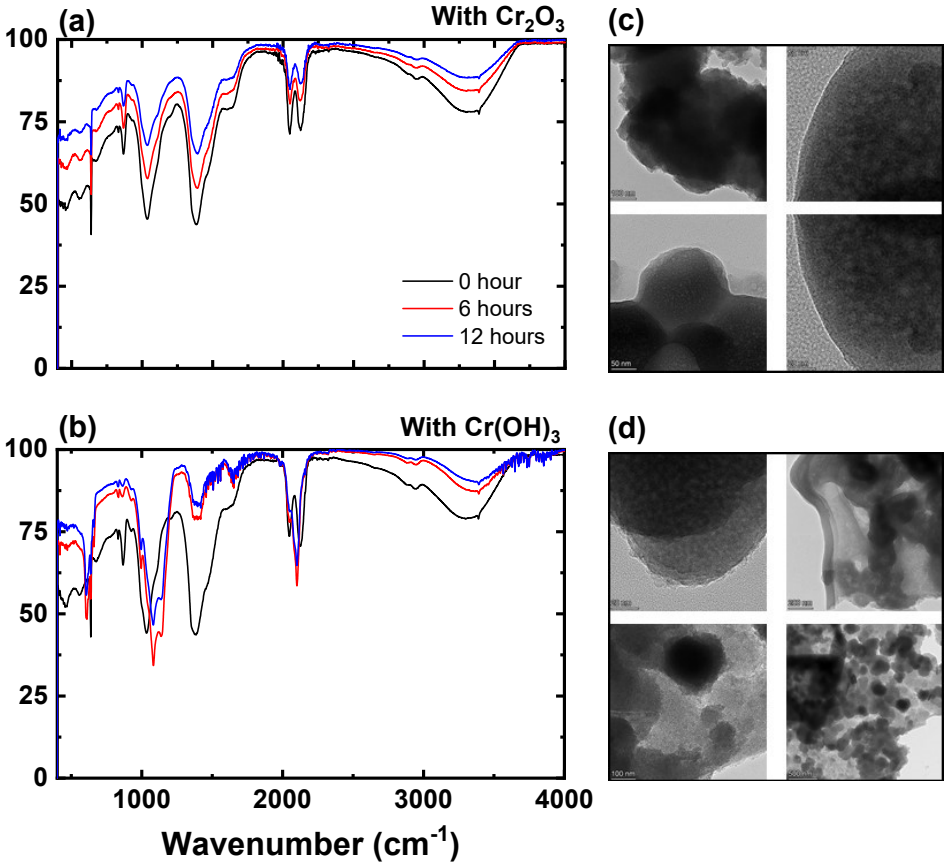

Figure S9 FTIR spectra of DOM in the presence of (a) Cr_2O_3 and (b) $Cr(OH)_3$. TEM images of (c) Cr_2O_3 and (b) $Cr(OH)_3$ in the presence of DOM.

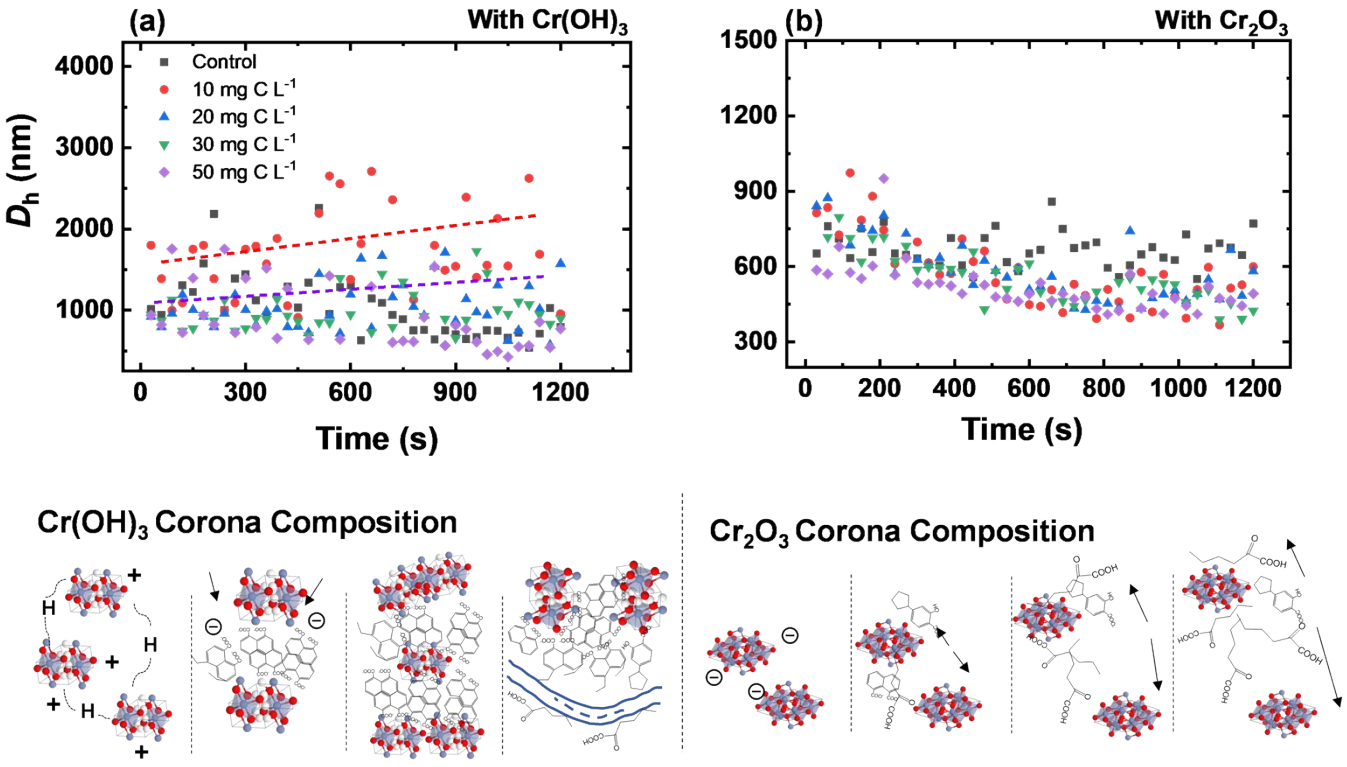

Figure S10 The dynamic changes in hydrodynamic diameters (nm) of (a) $Cr(OH)_3$ and (b) Cr_2O_3 under different DOM loadings (mg C L^{-1}). Schematic representation of corona formation of Cr (hydr)oxides and its impacts on the colloidal stabilities. The organic compound formulas were only shown to illustration.

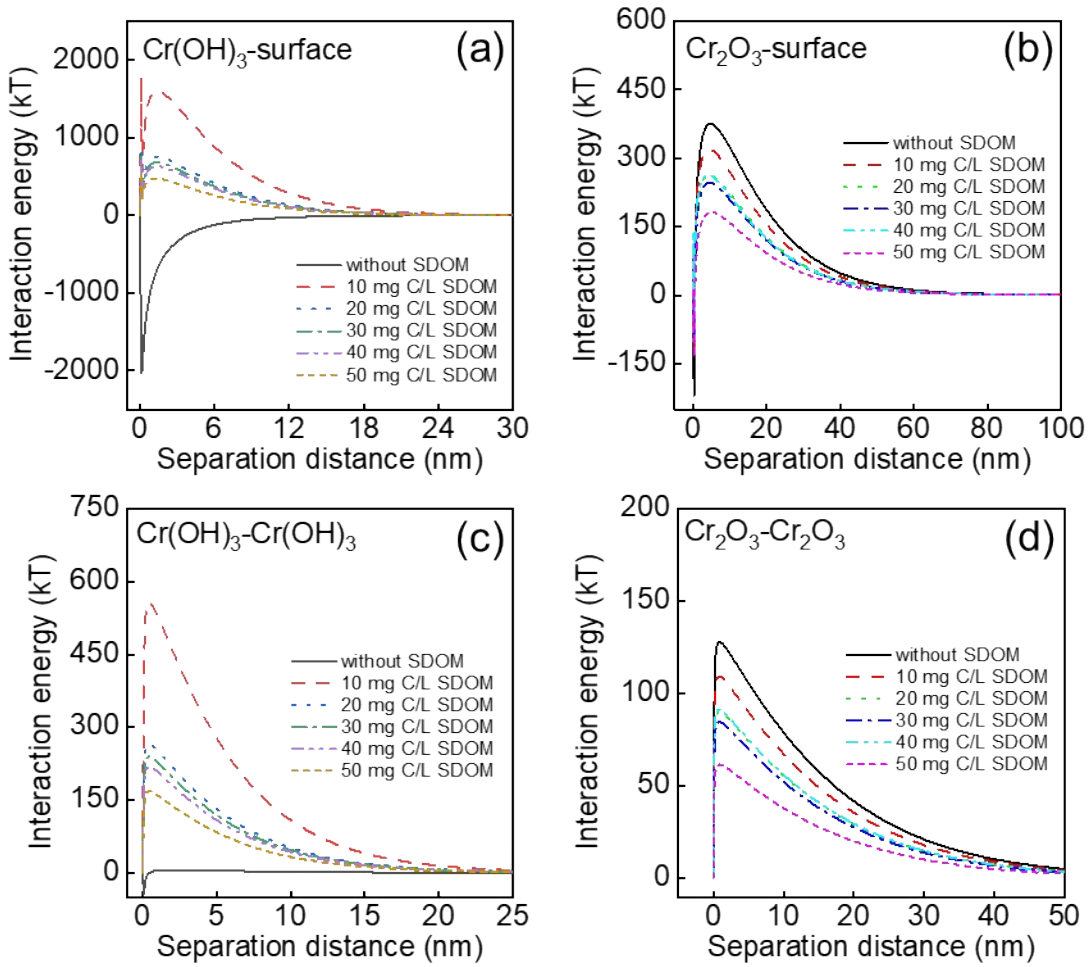

Figure S11 DLVO calculation profiles of Cr (hydr)oxide colloids with SDOM: (a-b) colloid-surface, (c-d) colloid-colloid.

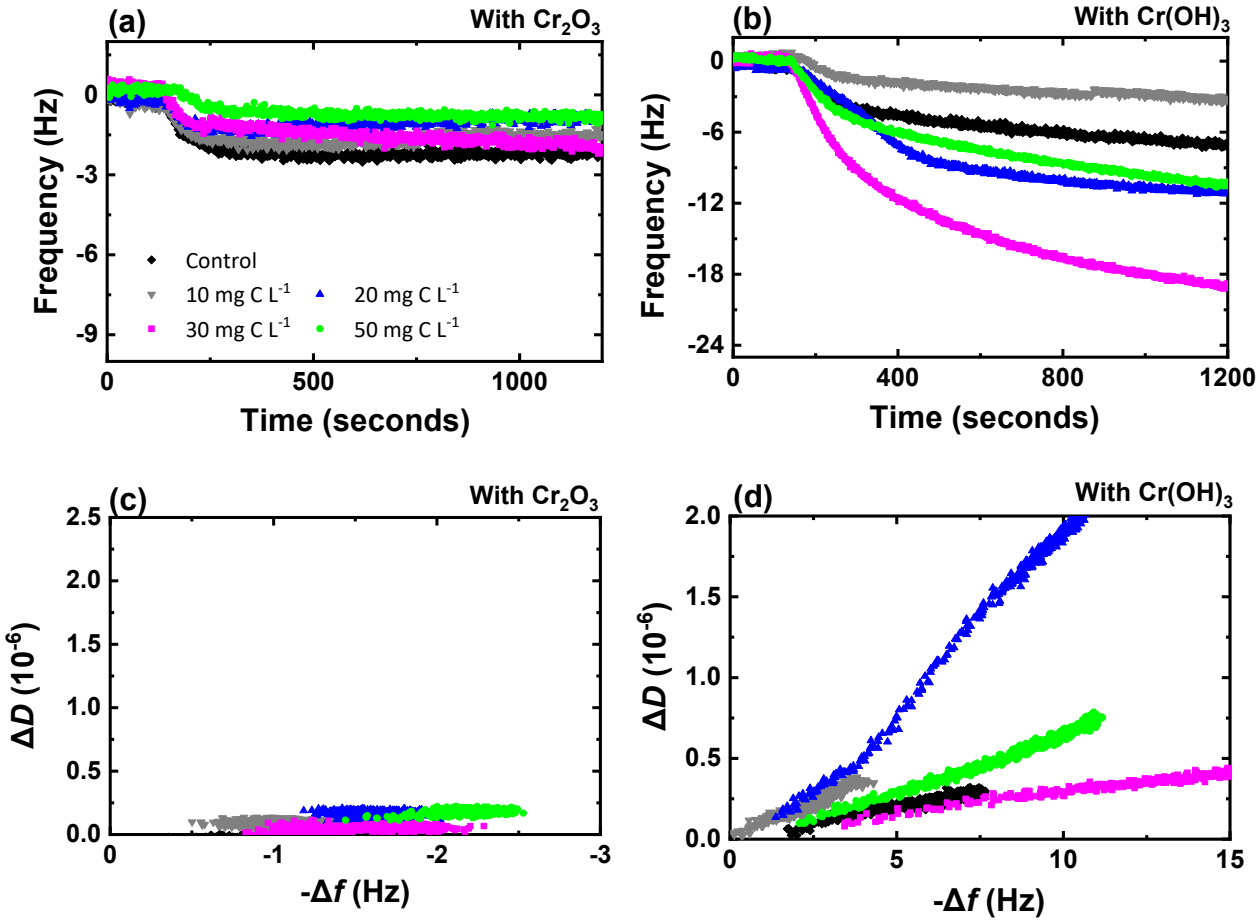

Figure S12 Deposition kinetics of Cr (hydr)oxide colloids with or without DOM detected in a QCM-D system.

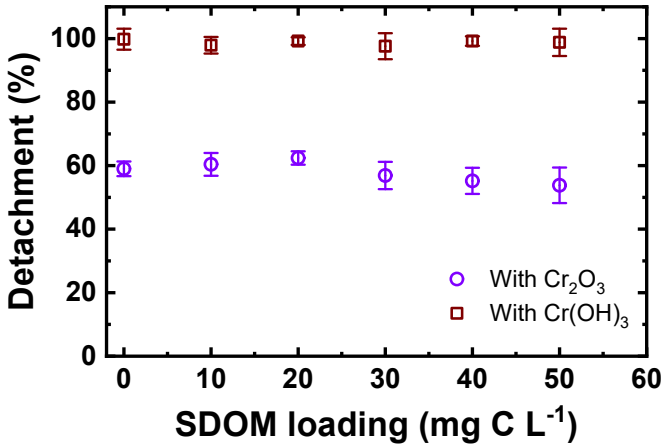

Figure S13. Deposition irreversibility (detachment efficiencies) (%) of $Cr(OH)_3$ and Cr_2O_3 in a QCM-D system as a function of DOM loadings (mg C L^{-1}).

References:

1. Lv, J.; Zhang, S.; Wang, S.; Luo, L.; Cao, D.; Christie, P., Molecular-scale investigation with ESI-FT-ICR-MS on fractionation of dissolved organic matter induced by adsorption on iron oxyhydroxides. *Environ. Sci. Technol.* **2016,** *50*, 2328-2336.
2. Zhang, T.; Li, C.; Ma, J.; Tian, H.; Qiang, Z., Surface hydroxyl groups of synthetic α-FeOOH in promoting OH generation from aqueous ozone: property and activity relationship. *Appl. Catal. B-Environ.* **2008,** *82*, 131-137.
3. Li, X.-M.; Sun, G.-X.; Chen, S.-C.; Fang, Z.; Yuan, H.-Y.; Shi, Q.; Zhu, Y.-G., Molecular chemodiversity of dissolved organic matter in paddy soils. *Environ. Sci. Technol.* **2018,** *52*, 963-971.
4. Ding, Y.; Shi, Z.; Ye, Q.; Liang, Y.; Liu, M.; Dang, Z.; Wang, Y.; Liu, C., Chemodiversity of soil dissolved organic matter. *Environ. Sci. Technol.* **2020,** *54*, 6174-6184.
5. Gu, B.; Schmitt, J.; Chen, Z.; Liang, L.; McCarthy, F., Adsorption and Desorption of Natural Organic Matter on Iron Oxide: Mechanisms and Models. *Environ. Sci. Technol.* **1994,** *28*, 38-46.
6. Mikutta, R.; Mikutta, C.; Kalbitz, K.; Scheel, T.; Kaiser, K.; Jahn, R., Biodegradation of forest floor organic matter bound to minerals via different binding mechanisms. *Geochim. Cosmochim. Ac.* **2007,** *71*, 2569-2590.
7. Yang, F.; Xu, Z.; Yu, L.; Gao, B.; Xu, X.; Zhao, L.; Cao, X., Kaolinite enhances the stability of the dissolvable and undissolvable fractions of biochar via different mechanisms. *Environ. Sci. Technol.* **2018,** *52*, 8321-8329.
8. Yuan, Z.-C.; Li, W.; Wu, L.; Huang, D.; Wu, M.; Hu, B., Solid-phase microextraction fiber in face mask for in vivo sampling and direct mass spectrometry analysis of exhaled breath aerosol. *Anal. Chem.* **2020,** *92*, 11543-11547.
9. Dittmar, T.; Koch, B.; Hertkorn, N.; Kattner, G., A simple and efficient method for the solid-phase extraction of dissolved organic matter (SPE-DOM) from seawater. *Limnol. Oceanogr- Meth.* **2008,** *6*, 230-235.
10. Cao, D.; Huang, H.; Hu, M.; Cui, L.; Geng, F.; Rao, Z.; Niu, H.; Cai, Y.; Kang, Y., Comprehensive characterization of natural organic matter by MALDI-and ESI-Fourier transform ion cyclotron resonance mass spectrometry. *Anal. Chim. Acta* **2015,** *866*, 48-58.
11. Kim, S.; Kramer, R. W.; Hatcher, P. G., Graphical method for analysis of ultrahigh-resolution broadband mass spectra of natural organic matter, the van Krevelen diagram. *Anal. Chem.* **2003,** *75*, 5336-5344.
12. Stenson, A. C.; Marshall, A. G.; Cooper, W. T., Exact masses and chemical formulas of individual Suwannee River fulvic acids from ultrahigh resolution electrospray ionization Fourier transform ion cyclotron resonance mass spectra. *Anal. Chem.* **2003,** *75*, 1275-1284.
13. Boye, K.; Noël, V.; Tfaily, M. M.; Bone, S. E.; Williams, K. H.; Bargar, J. R.; Fendorf, S., Thermodynamically controlled preservation of organic carbon in floodplains. *Nat. Geosci.* **2017,** *10*, 415-419.
14. Hughey, C. A.; Hendrickson, C. L.; Rodgers, R. P.; Marshall, A. G.; Qian, K., Kendrick mass defect spectrum: a compact visual analysis for ultrahigh-resolution broadband mass spectra. *Anal. Chem.* **2001,** *73*, 4676-4681.
15. Fleury, G.; Del Nero, M.; Barillon, R., Effect of mineral surface properties (alumina, kaolinite) on the sorptive fractionation mechanisms of soil fulvic acids: Molecular-scale ESI-MS studies. *Geochim. Cosmochim. Ac.* **2017,** *196*, 1-17.
16. Galindo, C.; Del Nero, M., Molecular level description of the sorptive fractionation of a fulvic acid on aluminum oxide using electrospray ionization Fourier transform mass spectrometry. *Environ. Sci. Technol.* **2014,** *48*, 7401-7408.
17. Sauerbrey, G. Verwendung von Schwingquarzen zur Wägung dünner Schichten und zur Mikrowägung. Zeitschrift. für. physic. **1959**, *155*, 206-222.
18. Zhang, M.; He, L.; Jin, X.; Bai, F.; Tong, M.; Ni, J. Flagella and their properties affect the transport and deposition behaviors of *Escherichia* coli in quartz sand. Environ. Sci. Technol. **2021**, *55*, 4964-4973.
19. He, L.; Li, M.; Wu, D.; Guo, J.; Zhang, M.; Tong, M. Freeze-thaw cycles induce diverse bacteria release

behaviors from quartz sand columns with different water saturations. Water Res **2022**, *221*, 118683.

20. Shen, C. Y.; Lazouskaya, V.; Jin, Y.; Li, B. G.; Ma, Z. Q.; Zheng, W. J.; Huang, Y. F. Coupled factors influencing detachment of nano- and micro-sized particles from primary minima. *J. Contam. Hydrol.* **2012**, *134*, 1-11.
21. Huang, X. F.; Bhattacharjee, S.; Hoek, E. M. V. Is surface roughness a "Scapegoat" or a primary factor when defining particle-substrate interactions? *Langmuir* **2010**, *26*, 2528-2537.
22. Bradford, S. A.; Torkzaban, S. Colloid interaction energies for physically and chemically heterogeneous porous media. *Langmuir.* **2013**, *29,* 3668-3676.
23. Ma, M.; Liu, R. P.; Liu, H. J.; Qu, J. H.; Jefferson, W. Effects and mechanisms of pre-chlorination on *Microcystis aeruginosa* removal by alum coagulation: Significance of the released intracellular organic matter. *Sep. Purif. Technol.* **2012**, *86*, 19-25.
24. Hogg, R.; Healy, T. W.; Fuerstenau, D. W. J. T. F. S. Mutual coagulation of colloidal dispersions. Trans. Faraday Soc. **1966**, *62*, 1638-1651.
25. Xia, T.; Lin, Y.; Li, S.; Yan, N.; Xie, Y.; He, M.; Guo, X.; Zhu, L. Co-transport of negatively charged nanoparticles in saturated porous media: Impacts of hydrophobicity and surface O-functional groups. *J. Hazard. Mater.* **2021**, *409*, 124477.
26. Gregory, J. Approximate expressions for retarded van der waals interaction. *J. Colloid Interface Sci.* **1981**, *83*, 138-145.
27. Bendersky, M.; Davis, J. M. DLVO interaction of colloidal particles with topographically and chemically heterogeneous surfaces. *J. Colloid Interface Sci.* **2011**, *353*, 87-97.
28. Ruckenstein, E.; Prieve, D. C., Adsorption and desorption of particles and their chromatographic separation. *AIChE J.*, **1976,** *22*, 276-283
29. Elimelech, M.; Gregory, J.; Jia, X.; Williams, R., Particle deposition and aggregation, measurement, modeling and simulation. *Colloid. Surf., A.*, **1997,** *1*, 93-94.
30. Elimelech, M.; O'Melia, C. R. Effect of particle size on collision efficiency in the deposition of Brownian particles with electrostatic energy barriers. *Langmuir* **1990**, *6*, 1153-1163.